Dikmese *et al. J Wireless Com Network* (2021) 2021:30
https://doi.org/10.1186/s13638-020-01889-w

EURASIP Journal on Wireless Communications and Networking

RESEARCH Open Access

Novel filter bank-based cooperative spectrum sensing under practical challenges for beyond 5G cognitive radios

Sener Dikmese*, Kishor Lamichhane and Markku Renfors

*Correspondence:
sener.dikmese@tuni.fi
Electrical Engineering, Faculty of Information Technology and Communication Sciences, Tampere University, Tampere, Finland

Abstract

Cognitive radio (CR) technology with dynamic spectrum management capabilities is widely advocated for utilizing effectively the unused spectrum resources. The main idea behind CR technology is to trigger secondary communications to utilize the unused spectral resources. However, CR technology heavily relies on spectrum sensing techniques which are applied to estimate the presence of primary user (PU) signals. This paper firstly focuses on novel analysis filter bank (AFB) and FFT-based cooperative spectrum sensing (CSS) techniques as conceptually and computationally simplified CSS methods based on subband energies to detect the spectral holes in the interesting part of the radio spectrum. To counteract the practical wireless channel effects, collaborative subband-based approaches of PU signal sensing are studied. CSS has the capability to relax the problems of both hidden nodes and fading multipath channels. FFT- and AFB-based receiver side sensing methods are applied for OFDM waveform and filter bank-based multicarrier (FBMC) waveform, respectively, the latter one as a candidate beyond-OFDM/beyond-5G scheme. Subband energies are then applied for enhanced energy detection (ED)-based CSS methods that are proposed in the context of wideband, multimode sensing. Our first case study focuses on sensing potential spectral gaps close to relatively strong primary users, considering also the effects of spectral regrowth due to power amplifier nonlinearities. The study shows that AFB-based CSS with FBMC waveform is able to improve the performance significantly. Our second case study considers a novel maximum–minimum energy detector (Max–Min ED)-based CSS. The proposed method is expected to effectively overcome the issue of noise uncertainty (NU) with remarkably lower implementation complexity compared to the existing methods. The developed algorithm with reduced complexity, enhanced detection performance, and improved reliability is presented as an attractive solution to counteract the practical wireless channel effects under low SNR. Closed-form analytic expressions are derived for the threshold and false alarm and detection probabilities considering frequency selective scenarios under NU. The validity of the novel expressions is justified through comparisons with respective results from computer simulations.

Keywords: Cognitive radio, Cooperative spectrum sensing, AFB-based ED, Power amplifier nonlinearity, Max–Min ED

1 Introduction

With the growing attention on wireless communications, radio spectrum scarcity has become modern days' challenge. Higher demand of spectral bandwidth is pushing spectrum usage to utmost limits. However, the limitations of traditional wireless technology lead to spectrum wastage, inviting opportunistic usages of those valuable unused resources [1]. These studies have mainly focused on technologies that solve the problem of spectral scarcity by using opportunistically the frequency band to establish secondary communication. Such technology is commonly known as cognitive radio (CR) technology, which defines new dimension to the modern communication systems advocating environment-adaptive radio transmission [2]. CR keeps track of the radio transmission environment continuously, while it dynamically varies its transmission parameters so as to adjust its operation to the surroundings.

Spectrum sensing-based CR technology is considered as highly interesting topic in wireless communications. Spectrum sensing, in other words, involves tracking of the PU activity so as to estimate the spectral holes. Different sensing algorithms find the availability of spectral holes as an opportunity to enable the secondary communication [3]. Recent studies have suggested a wide variety of spectrum sensing techniques, but none of them is fully satisfying in terms of all relevant metrics like implementation complexity, reliability, and loss in secondary system throughput. Especially, spectrum sensing under low signal-to-noise ratio (SNR) is widely covered in the literature, under conditions where the noise dominates the weak PU signal [3, 4]. Under these conditions, the spectrum sensing becomes critically sensitive to imperfect knowledge of the power and characteristics of noise and interferences [5–7].

Spectrum that is originally assigned to the PU can be used by a secondary user (SU) if and only if the PU becomes idle. Since SUs can only use spectrum as an opportunity in terms of the spectrum sharing, spectrum sensing has a great role to play in CR technology [3, 8]. Regarding the importance of the radio scene analysis function, basic spectrum sensing methods show numerous limitations. Shadowing, hidden node problems, etc., always make spectrum sensing challenging. A PU transmission may be unobservable for a CR sensing station, while its signal is fully usable by a nearby PU receiver. In order to make the spectrum sensing function reliable, efficient, and to counteract both multipath and hidden node problems, cooperative spectrum sensing (CSS) is considered as a vital solution especially in wideband situations. CSS involves two or more cooperative radio receivers in decision making during spectrum sensing. Collaboration among number of CR users to enhance the detection performance was suggested in [9].

Wideband sensing approaches are applied over multiple PU channels in an efficient way, which is highly desirable to increase the probability of determining unoccupied spectrum bands. Cooperative wideband spectrum sensing under fading channels has been recently proposed in the literature [10–13]. These approaches not only provide computation and memory savings compared to the existing wideband spectrum sensing methods, but also reduce the hardware requirements and the energy costs at CRs [10–13].

Our studies further exploit the collaborative approach of spectrum sensing. The studies of this paper firstly focus on subband-based spectrum sensing methods that add the collaboration among a number of CR receivers to enhance the sensing performance and

to counteract practical wireless channel effects. In the first part of current study, we develop the ideas that we presented in [14] under more practical situations and study the performance of our algorithms in more details. CSS exploits the diversity among a number of CR receivers having different multipath channel profiles and experiencing different large-scale fading (shadowing) characteristics towards the PU transmissions [15].

Moreover, maximum–minimum energy detector (Max–Min ED) has been found to be a robust and effective non-cooperative spectrum sensing scheme [6, 7]. This approach applies subband decomposition of the received signal and the difference of maximum and minimum subband energies as a test statistic. This method has been shown to provide acceptable performance at the low SNR regime with noise uncertainty (NU) [6, 7]. The intuitive simplistic idea behind these approaches is that in certain scenarios, the minimum subband energy can be regarded as an estimate for the noise variance. Moreover, the presence of a PU signal introduces frequency variability of the received power spectral density (PSD), which is not critically affected by the NU. Based on the above, it becomes evident that subband detection is capable of mitigating the NU effects. To the best of the authors' knowledge, this approach has not been considered in the context of CSS. Hence, in this study we present a highly accurate and robust CSS method with reduced computational complexity utilizing the Max–Min ED approach.

More specifically, the contributions of this paper are listed below:

- Conceptually and computationally simplified CSS methods based on subband energies are developed. Subband energies are evaluated either using fast Fourier transform (FFT) or analysis filter bank (AFB). Subband-based CSS methods are proposed in the context of wideband, multimode sensing employing FFT or filter bank methods for the required spectrum analysis procedures. These approaches can be applied in wideband heterogeneous dynamic spectrum use scenarios, where different kinds of PUs and SUs can coexist.
- CSS methods are applied to ideal OFDM waveform in most of the studies in the literature. In the proposed study, subband ED-based CSS methods are applied on the traditional OFDM as a reference model and on filter bank multicarrier (FBMC) waveforms, the latter one as a candidate beyond-OFDM/beyond-5G scheme.
- The effects of both power amplifier (PA) nonlinearities and practical wireless channels on subband ED-based CSS are investigated, comparing the performance of FFT- and AFB-based CSS schemes. The most critical issue in this context is the spectral regrowth due to the nonlinear PA of the PU transmitter. While FBMC/OQAM has superior spectral containment, AFB on the receiver side improves the resolution of spectrum sensing, making it possible to detect potential narrowband PUs in the targeted sensing band.
- A novel Max–Min ED-based CSS is proposed and found to be robust to NU, providing better performance than traditional CSS with significantly less complexity compared to the advanced eigenvalue-based sensing approaches [7]. The proposed Max–Min ED-based approaches have also lower computational complexity compared to the differential Max–Min ED [16] considered as an alternative reference model, which is included in the performance comparisons of this paper.

- Novel analytic models for energy threshold and false alarm and detection probabilities are derived considering frequency selective scenarios under NU. The offered results are validated extensively through comparisons with respective computer simulations. These results provide meaningful insights that are for future beyond-OFDM/beyond-5G design and deployments of CR communication systems and networks.

1.1 Overview and methods

In this study, two novel approaches (i) *subband FFT- and AFB-based CSS* and (ii) *Max–Min ED-based CSS* are proposed in the context of spectrum sensing. In the study of subband-based CSS, traditional OFDM and FBMC waveforms (beyond-OFDM/beyond-5G scheme) are considered under PA nonlinearity and practical frequency selective channel with log-normal shadowing model.

The remainder of the paper is organized as follows: Sect. 2 gives a general idea about traditional CSS methods. Novel FFT- and AFB-based CSS methods are presented in Sect. 3. Also, signal models including PA nonlinearities, frequency-selective fading, and shadowing for FFT- and AFB-based CSS are described in the same section. Novel Max–Min ED-based CSS with its detailed analytical model is presented in Sect. 4. Numerical results for sensing performance are shown in Sect. 5. These include comparisons between the analytical model and performance results that are obtained through Monte Carlo simulations based on a developed MATLAB script. Finally, closing remarks are given in Sect. 6.

2 Traditional cooperative spectrum sensing

Practical wireless channels show characteristics like NU, multipath fading, and shadowing. In order to mitigate the effects of practical wireless channels, cooperation among many CR users, i.e., CSS is considered. CSS is regarded as a potential solution to mitigate effects of both multipath and shadowing which causes the hidden node problem [9]. It also enhances the detection performance and reliability [4]. Spatial diversity among multiple receivers is achieved, as illustrated in Fig. 1. The concept of exploiting SUs' spatial diversity to counteract the hidden node effects and enabling cooperation among SUs is coined as CSS and has reached growing attention in recent years.

CSS uses two or more spatially separated CR receivers to combine their sensing results so as to increase the reliability of the sensing decision. Combining the results from different CR receivers is performed at the fusion center (FC) [17, 18]. Different rules may be considered for combining the individual sensing results in order to achieve the highest accuracy at the FC, depending on the radio environment. With an increase in the number of CR users, the CSS procedure becomes more complicated. On the other hand, with increased number of CR receivers, the sensing performance enhances significantly, considering performance parameters like sensing time and reliability. So there is a trade-off between sensing performance and complexity of the CSS system. It is noted that based on experimental tests, the number of sensors is selected as 8 in our study. When the number of sensors is decreased, the performance of the sensing is significantly degraded.

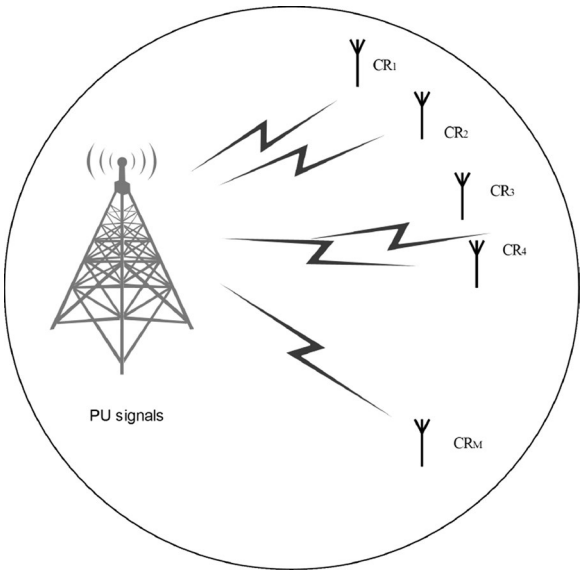

Fig. 1 CR topology including a PU transmitter and *M* CR stations

With higher number of sensing stations, the performance was not significantly improved in our simulation scenarios. However, in practice this depends on the geographical distribution of the sensors.

Cooperative schemes can be classified as hard and soft fusion schemes. When CRs provide binary information about the presence of PUs, the FC applies hard fusion rules. If the CRs may provide reliability information about their sensing results in the form of non-binary soft decisions, the FC applies a soft fusion scheme [18]. Our studies consider the ED-based CSS approach with hard decision combining.

2.1 Hard decision fusion with linear fusion rules

Hard fusion can be implemented using linear rules such as *AND rule*, *OR rule*, or *Majority rule*. Hard decision fusion does not need to exchange data among secondary nodes. Soft schemes generally improve the sensing result by sending richer information to the FC. Soft fusion techniques increase the complexity compared to hard fusion techniques. Linear fusion rules are commonly applied by the FC to exploit the cooperation among CR receivers. Binary decision from independent CR receivers is forwarded to the FC. FC processes the decisions from all CRs to make the collective decision. Linear fusion rules are based on the general *k-out-of-M rule* [18, 19].

2.1.1 OR rule

is one of the fusion rules which is applied at FC. When at least one SU detects the PU signal, *OR rule* declares the presence of PU. With M SUs, the cooperative detection probability $P_{D,t}$ and false alarm probability $P_{FA,t}$ after the decision at the FC are computed as follows:

$$\text{OR-Rule}: \begin{cases} P_{D,t} = 1 - (1 - P_D)^M \\ P_{FA,t} = 1 - (1 - P_{FA})^M \end{cases}. \tag{1}$$

Here, P_D and P_{FA} are the detection and false alarm probabilities of individual SUs reported to the FC, which are assumed to be equal for all CR stations.

2.1.2 AND rule

declares the presence of a PU signal if and only if all SUs detect the PU signal individually. With M SUs, the cooperative detection probability $P_{D,t}$ and false alarm probability $P_{FA,t}$ at a FC are computed as follows:

$$\text{AND Rule}: \begin{cases} P_{D,t} = {P_D}^M, \\ P_{FA,t} = P_{FA}^M. \end{cases} \tag{2}$$

2.1.3 Majority rule

According to various studies, both *AND rule* and *OR rule* are limited in terms of detection and false alarm probabilities. *Majority rule* is another case of the generalized *k*-out-of-*M rule*. If at least half of the SUs report the presence of PU, FC declares the presence of PU, otherwise it declares that the spectrum is free to use for CR transmission [15, 17]. Considering an even number M of sensing stations in the CSS, the cooperative detection and false alarm probabilities of the *Majority rule* can be written as follows:

$$M/2+1 \text{ -out-of- } M: \begin{cases} P_{D,t} = \sum_{j=M/2+1}^{M} \binom{M}{j} P_D^j \cdot (1 - P_D)^{M-j} \\ P_{FA,t} = \sum_{j=M/2+1}^{M} \binom{M}{j} (1 - P_{FA})^{M-j} \cdot P_{FA}^j. \end{cases} \tag{3}$$

2.1.4 Generalized k-out-of-M rule

The generalized form of the linear rule can be defined by requiring k SUs out of M to report the presence of a PU signal. Here the number k can take any value between 1 and M, based on the requirements. As discussed earlier, the special cases $k = 1$, $k = M/2 + 1$, and $k = M$ are equivalent to *OR rule*, *Majority rule*, and *AND rule*, respectively. Nevertheless, the number k can be optimized according to the targeted detection and false alarm performance [17, 19]. The cooperative detection and false alarm probabilities of this rule are as follows:

$$K_{of}N: \begin{cases} P_{D,t} = \sum_{j=k}^{M} \binom{M}{j} P_D^j \cdot (1 - P_D)^{M-j} \\ P_{FA,t} = \sum_{j=k}^{M} \binom{M}{j} (1 - P_{FA})^{M-j} \cdot P_{FA}^j. \end{cases} \tag{4}$$

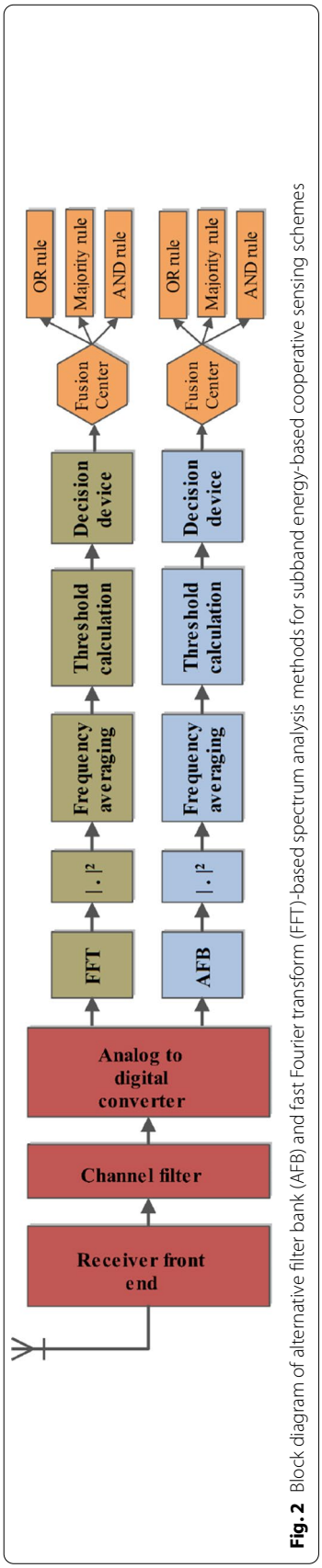

Fig. 2 Block diagram of alternative filter bank (AFB) and fast Fourier transform (FFT)-based spectrum analysis methods for subband energy-based cooperative sensing schemes

3 Novel FFT- and AFB-based cooperative spectrum sensing

FFT- and AFB-based techniques are applied to a wideband signal to generate equally spaced subband signals. Subband energies are then calculated and the subband energy detector (SED) decides on the presence of PU signal(s) within the processed frequency band based on the subband energies [3, 5, 7]. The entire procedure is represented in Fig. 2. The receiver front-end collects the PU signals which are followed by a channel filter and analog-to-digital converter (ADC). The subband signals can be obtained either via FFT or AFB and then processed accordingly [5].

3.1 Subband-based sensing

A subband signal can be represented as follows,

$$Y_k[m] = \begin{cases} \mathcal{W}_k[m] & \mathcal{H}_0, \\ S_k[m]H_k + \mathcal{W}_k[m] & \mathcal{H}_1. \end{cases} \tag{5}$$

Here, $S_k[m]$ is the transmitted signal by PU as it appears at the mth FFT or AFB output sample in subband k and $\mathcal{W}_k[m]$ is the corresponding channel noise sample. $\mathcal{H}_1$ denotes the *present hypothesis* of a PU signal whereas $\mathcal{H}_0$ denotes the *absent hypothesis* of a PU signal. When the AWGN only is present, the white noise is modeled as a zero-mean Gaussian random variable with variance σ_w^2, i.e., $\mathcal{W}_k[m] = \mathcal{N}(0, \sigma_w^2)$. The OFDM and FBMC signals can also be modeled in terms of zero-mean Gaussian variables, $S_k[m] = \mathcal{N}(0, \sigma_k^2)$, where σ_k^2 is the variance (power) at subband k. The subband energy is calculated from the subband signals of Eq. (5). The integrated test statistics to be used in the SED process is calculated as

$$T(y_{m0}, k_0) = \frac{1}{N_t N_f} \sum_{k=k_0-[N_f/2]}^{k_0+[N_f/2]-1} \sum_{m=m_0}^{m_0+N_t+1} |y_k[m]|^2. \tag{6}$$

Here, N_f and N_t are the averaging window lengths in frequency and time domains, respectively. Assuming flat PU spectrum over the sensing band, the probability distribution of the test statistics can be expressed as

$$T(y_{m0}, k_0)|\mathcal{H}_0 \sim \mathcal{N}\left(\sigma_{w,k}^2, \frac{\sigma_{w,k}^4}{N_t N_f}\right) \tag{7}$$

and

$$T(y_{m0}, k_0)|\mathcal{H}_1 \sim \mathcal{N}\left(\sigma_{x,k}^2 + \sigma_{w,k}^2, \frac{\left(\sigma_{x,k}^2 + \sigma_{w,k}^2\right)^2}{N_t N_f}\right). \tag{8}$$

This yields

$$P_{FA} = P_r(T(y) > \lambda|\mathcal{H}_0) = Q\left(\frac{\lambda - \sigma_{w,k}^2}{\sigma_{w,k}^2/\sqrt{N_f N_t}}\right) \tag{9}$$

and

$$P_D = P_r(T(y) > \lambda|\mathcal{H}_1) = Q\left(\frac{\lambda - \sigma_{w,k}^2(1+\gamma_k)}{\sigma_{w,k}^2(1+\gamma_k)/\sqrt{N_f N_t}}\right). \tag{10}$$

Here, $\gamma_k = \sigma_{x,k}^2/\sigma_{w,k}^2$ is the SNR of subband k and $\sigma_{w,k}^2 = \sigma_w^2/N_{FFT}$ and $\sigma_{x,k}^2$ denote noise variance and the PU signal variance in subband k, respectively.

Applying FFT- or AFB-based processing and adjusting the averaging window in frequency, it is possible to tune the sensing frequency band for a specific PU channel while maximizing the sensitivity of the sensing process. Limited number of possible PU channels with different bandwidths and center frequencies can be handled by having parallel integration processes for each of candidate channels, based on a common FFT or AFB module. Alternatively, sensing decisions can be done blindly, without knowledge of the PU channel raster, by integrating the test statistics for fixed equally-spaced subbands. Obviously, such approach is sensitive to frequency-selective fading effects, and the diversity provided by CSS would greatly improve the reliability of such schemes. In such cases, the required averaging window length in time depends on the subband width and targeted sensitivity of sensing. In this way, multiple center frequencies, bandwidths, and multiple spectral gaps can be identified rapidly, efficiently, and flexibly for potential use by the CR.

For given P_{FA}, the threshold λ can be calculated as

$$\lambda = \sigma_{w,k}^2\left(1 + \frac{Q^{-1}(P_{FA})}{\sqrt{N_f N_t}}\right). \tag{11}$$

3.2 Waveforms and spectrum sensing schemes

OFDM with cyclic prefix, i.e., CP-OFDM, is the dominating multicarrier technology in the field of wireless communications. Additionally, discrete wavelet multitone (DWMT), cosine modulated multitone (CMT), filtered multitone (FMT), and OFDM with offset-QAM (OFDM/OQAM, also known as FBMC/OQAM) are commonly considered alternative forms of multicarrier techniques [20]. FBMC waveforms, especially FBMC/OQAM have been widely considered as candidates for beyond-OFDM multicarrier systems. It is particularly suitable for dynamic opportunistic spectrum use and CR [21]. FBMC/OQAM shows better spectral efficiency compared to CP-OFDM. Such FBMC/OQAM systems utilize a signal model with real valued symbol sequence at twice the QAM symbol rate, instead of complex QAM symbols. Polyphase filter banks in transmultiplexer configuration constitute the core elements of the transmission link. Specifically, synthesis filter bank (SFB) and AFB are used at the transmitter and receiver sides, respectively [3, 5].

On the receiver side, the FFT of an OFDM receiver or AFB of an FBMC receiver can be used also for spectrum sensing purposes, providing SED capability without additional processing elements. Subband-based ED can be used in wideband spectrum sensing which covers multiple PU frequency channels or even the whole service band. For FBMC, the PHYDYAS prototype filter with overlap factor $K = 4$ [3] is used in our study. Such filter bank reaches about 50 dB stopband attenuation, providing efficient detection of narrow spectral gaps between PU channels [20, 21].

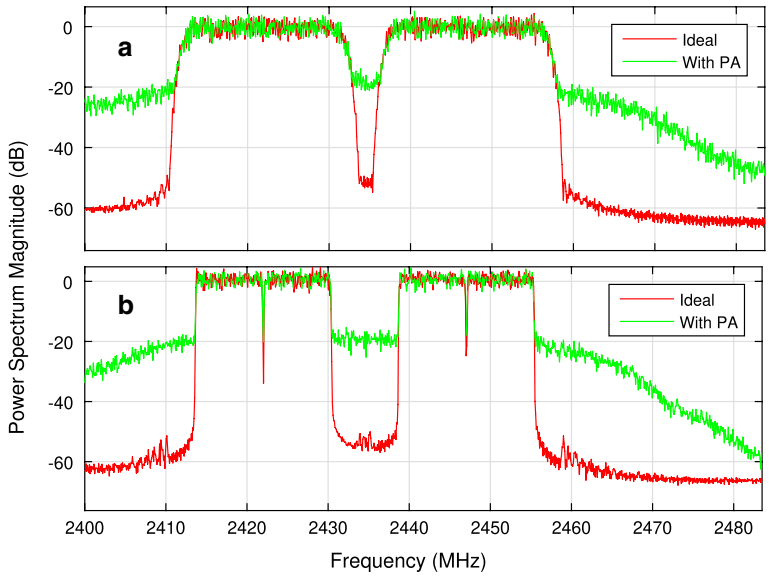

Fig. 3 Effects of the PA model on **a** OFDM and **b** FBMC-based PU spectra. A Wiener behavioral model with fifth order nonlinearity and 5 dB backoff is used for the PA

In the following, we consider two scenarios: (i) sensing CP-OFDM signal using FFT-based SED and (ii) sensing FBMC/OQAM signal using AFB-based SED. The two waveforms have the same number of active subcarriers with common subcarrier spacing.

3.3 Power amplifier model for PUs

Various interference leakage effects due to RF imperfections affect critically the spectrum sensing performance in practice. The most significant issue in this context is the spectral regrowth due to the nonlinear PA of the PU transmitter. For a practical PA model, we consider the linear time-invariant (LTI) portion of the Wiener PA model, which has a pole/zero form of the system function given by [3]

$$H(z) = \frac{1 + 0.3z^{-2}}{1 - 0.2z^{-1}}. \tag{12}$$

This is extracted from an actual Class AB PA with fifth order nonlinearity. In this study, 5 dB backoff is assumed with this PA model.

The potential spectral hole between two relatively strong PUs is shown in Fig. 3 for both scenarios, as determined by the corresponding sensing process, i.e., FFT for CP-OFDM and AFB for FBMC. While FBMC/OQAM has superior spectral containment, AFB on the receiver side enhances the resolution of spectrum sensing, making it possible to detect potential narrowband PUs within the sensing band.

In theory, considering Gaussian approximation, it is possible to model the effect of PU transmitter's spectral leakage due to the PA nonlinearity on the actual false alarm probability $\tilde{P}_{FA}$ as follows:

$$\tilde{P}_{FA}(k) = Q\left(\frac{\lambda - \left(\sigma_{w,k}^2 + I_{adj}(k)\right)}{\sqrt{\frac{1}{N_f N_t}}\left(\sigma_{w,k}^2 + I_{adj}(k)\right)}\right) \tag{13}$$

where,

$$I_{adj}(k) = \int_{f_1}^{f_2} \left|H_2(f)\right|^2 \psi_{PA}(f) df \tag{14}$$

corresponds to the leakage power from the adjacent PU transmitter with out-of-band emission spectrum $\psi_{PA}(f)$ to the sensing frequency band between frequencies f_1 and f_2. $H_2(f)$ is the channel frequency response from a primary transmitter to the CR receiver. In (11), the threshold value λ is calculated using the traditional well-known analytical model from estimated noise variance and desired false alarm probability P_{FA}. Similarly, the detection probability $\tilde{P_D}$ can be expressed as follows

$$\tilde{P_D}(k) = Q\left(\frac{\lambda - \left(\left(\sigma_{w,k}^2 + I_{adj}(k)\right) + \sigma_{x,k}^2\right)}{\sqrt{\frac{1}{N_f N_t}}\left(\left(\sigma_{w,k}^2 + I_{adj}(k)\right) + \sigma_{x,k}^2\right)}\right). \tag{15}$$

In the case of reliable estimate of the PU's emission spectrum shape, the above analysis could be used for improving the spectrum sensing at the frequencies affected by the spectrum leakage. However, this is very difficult in practice due to the unpredictability of the PA characteristics, and the above model is used only for the purpose of performance analysis.

3.4 Channel model

This study applies frequency selective multipath channel model together with log-normal shadowing model. All PU and CR channels use *Indoor* frequency selective channel model having 90 ns RMS delay spread with 16 taps [22].

The log-normal path loss is modeled as follows:

$$PL = PL_0 * \left(\frac{d_j}{d_0}\right)^a * \varphi, \tag{16}$$

or in dB scale as,

$$PL_{dB} = PL_{0dB} + 10 * a * log(d_j/d_0) + \varphi_{dB}. \tag{17}$$

Here, PL_0 is the path-loss at the reference distance d_0, a represents the path-loss exponent, d_j represents the distance of jth CR receiver, and φ represents the shadow fading with Gaussian distribution, zero mean, and standard deviation σ.

We consider the two scenarios mentioned above, while the CR waveform is always FBMC. For log-normal fading $\sigma = 9$ dB and the path-loss exponent $a = 2$.

4 Novel maximum–minimum energy detection-based cooperative spectrum sensing

In this section, the novel Max–Min ED-based CSS method is proposed. This sensing technique, considered earlier only basic single-station sensing, is robust to the NU and yet reduces the complexity in comparison with existing methods with such robustness. The proposed sensing techniques outperform the other advance spectrum sensing methods under NU condition.

A matter of primary interest is to design algorithms that can deliver acceptable spectrum sensing performance with reduced complexity and reliability in terms of detection and false alarm performance. Existing spectrum sensing techniques are not satisfying in this respect. Particularly, sensing in low SNR range, i.e., (− 25 dB, − 10 dB), is challenging due to the noise susceptibility issues and the hidden node problem also exists. To counteract these issues, the spectrum sensing technique has to be more robust to NU, while exhibiting realistic computational complexity for practical implementation. In this section, a novel cooperative Max–Min ED scheme is proposed which reduces complexity and NU. Literature in [7, 16] covers the idea of the frequency diversity gain exploitation with the help of the statistics of the energy spectral density (ESD). Differentiation stage is suggested in the literature as a solution to the NU. However, studies in our group have proposed a solution without the differentiation stage, while maintaining the robustness to NU and exhibiting reduced computational complexity. Results show that the proposed solution outperforms the traditional ED and other detection algorithms. Figure 4 shows the steps implemented in different variants of the Max–Min ED algorithm.

4.1 Proposed Max–Min ED-based CSS method

In this subsection, an enhanced Max–Min ED method is considered, which is less complex than existing methods which are robust to NU. Illustration of the methods is as seen in Fig. 4. The maximum and minimum energies of the subbands are utilized for constructing the decision statistics. These statistics are used to estimate the presence and absence of PU. Actually, we consider here three alternative schemes, which are utilizing the subband energies in a different manner [6, 7]. These methods consist of following steps:

- SED to calculate subband energies,
- Ordering of the determined subband energies,
- Differentiation of the ordered subband energy sequence,
- Quantification of the maximum and minimum energies level,
- Calculation of a threshold and the implementation of decision device.

The proposed method removes the ordering and differentiation blocks from Fig. 4. Hence, the proposed method is less complex yet outperforms the other sensing methods.

The FFT operation on blocks of N_{FFT} input samples is applied. Alternatively, AFB with N_{FFT} subbands can be used and this choice is preferred in high dynamic range scenarios. The subband signals are formulated as in Eq. (5). Frequency variability of ESD is

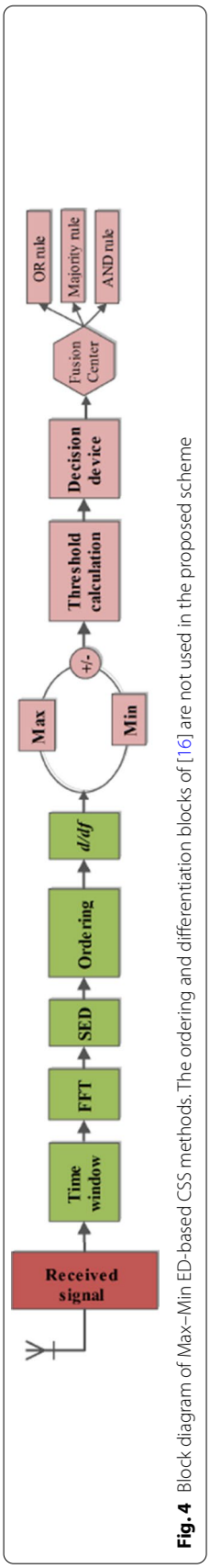

Fig. 4 Block diagram of Max–Min ED-based CSS methods. The ordering and differentiation blocks of [16] are not used in the proposed scheme

featured in Max–Min ED algorithms as depicted in Fig. 4 and the process is summarized as, $U_k = \frac{1}{L_t}\sum_{m=1}^{L_t}|Y_k[m]|^2$, where $L_t = N/N_{FFT}$ represents length of the window. From the central limit theorem, U_k for both $\mathcal{H}_0$ and $\mathcal{H}_1$ hypotheses is expressed as,

$$U_k = \begin{cases} \mathcal{N}\left(\sigma_{w,k}^2, \frac{2}{L_t}\sigma_{w,k}^4\right), & \mathcal{H}_0 \\ \mathcal{N}\left(|H_k|^2\sigma_{x,k}^2 + \sigma_{w,k}^2, \frac{2}{L_t}\left(|H_k|^2, \sigma_{x,k}^2 + \sigma_{w,k}^2\right)^2\right). & \mathcal{H}_1 \end{cases} \tag{18}$$

Maximum and minimum energies are estimated as depicted in Fig. 4 and the test statistics is calculated from the energy values. Test statistic is then compared with a predetermined threshold that is obtained from the target P_{FA} with the aid of Gumbel distribution. The presence and absence status of the PU signal is determined by comparing the threshold and test statistics. Analytical approach to calculate the thresholds will be given later in Sect. 4.2.

It is noted that differential subband energy-based scheme in [16] utilizes the following additional steps upon knowledge of the subband energies:

* *Ordering*: This step requires placing of the subband energies in the order of magnitude. This has no effect on the statistical properties of the ordered sequence, $\widehat{U}_k$, which follows the distribution in (18).
* *Differentiation*: The ordered subband energy sequence is differentiated such that $D_k = \widehat{U}_{k+1} - \widehat{U}_k$. This operation can be interpreted as a subtraction of two normally distributed random variables, as shown in (18), yielding

$$D_k \simeq \begin{cases} \mathcal{N}\left(0, \frac{4}{L_t}\sigma_{w,k}^4\right), & \mathcal{H}_0 \\ \mathcal{N}\left(E[\widehat{U}_k] - E[\widehat{U}_{k-1}], \frac{4}{L_t}\left(|H_k|^2\sigma_{x,k}^2 + \sigma_{w,k}^2\right)^2\right). & \mathcal{H}_1 \end{cases} \tag{19}$$

Under $\mathcal{H}_0$ hypothesis, the above expression yields a normal distribution with zero mean and twice the variance in (18). It is also noted that when the observed PU is white, the mean value reduces to zero and all subband energies follow a zero-mean Gaussian distribution also under $\mathcal{H}_1$ hypothesis. As a consequence, the algorithm fails to sense the PU.

The energy threshold γ is calculated as in the simplified method. Finally, if $D_{max} - D_{min} > \gamma$, the PU signal is assumed present, otherwise only noise is assumed present.

In terms of the computational complexity, the ordering and differentiation steps in the differentiation-based approach bring additional $\mathcal{O}(N_{FFT})$ and $\mathcal{O}(N_{FFT})$ complexities, respectively, compared to our proposed simplified method.

4.2 Analytical models for Max–Min-based energy detector

In this section, novel analytic expressions for the Max–Min ED-based CSS are formulated. Later, the derived analytical results are compared to simulation results, and a very good match is found between them [7].

4.2.1 Probability of false alarm and energy threshold

Recalling earlier studies, the test statistics depend on the maximum and minimum values of U_k. The statistics of maximum and minimum distribution is characterized by the von Mises theorem [7]. Following these statistics, the Gumbel distribution [23] is used for efficient representation of the extreme values of an arbitrary distribution namely,

$$f_{min}(x) = \frac{1}{\beta} e^{\frac{x-\alpha}{\beta}} e^{-e^{\frac{x-\alpha}{\beta}}} \tag{20}$$

and

$$f_{max}(x) = \frac{1}{\beta} e^{-\frac{x-\alpha}{\beta}} e^{-e^{-\frac{x-\alpha}{\beta}}} \tag{21}$$

here α and β represent the location and scale parameters of the distribution. The expected value and standard deviation of the difference of maximum and minimum values are derived from Eqs. (20) and (21), respectively. Based on the above equation and earlier studies of our group [7], both detection and false alarm probabilities for each sensing station are formulated as Eqs. (23) and (25), respectively.[1]

Using Gumbel distribution with mean and variance values of U_k in (18) for the $\mathcal{H}_0$ hypothesis one obtains

$$\begin{aligned} U_{\max-\min}|\mathcal{H}_0 &\sim \mathcal{Q}_{\mathcal{G}}\left(\alpha|_{\mathcal{H}_0}, \beta|_{\mathcal{H}_0}\right) \\ &\sim \mathcal{Q}_{\mathcal{G}}\left(\frac{\sigma_{w,k}^2}{2} + C\sqrt{\frac{6}{L_t}}\frac{\sigma_{w,k}^2}{\pi}, \sqrt{\frac{6}{L_t}}\frac{\sigma_{w,k}^2}{\pi}\right) \end{aligned} \tag{22}$$

where $\mathcal{Q}_G(\alpha, \beta)$ denotes the Gumbel distribution and $C = 0.577215665$ is the Euler's constant. The standard Gumbel complementary distribution function is given by $\mathcal{G}\left(\frac{x-\alpha}{\beta}\right) = 1 - e^{-e^{-\frac{x-\alpha}{\beta}}}$ [23–29].

In the practical environment, both expressions P_{FA} and P_D have to consider the NU. It is recalled that the noise distribution is summarized in the range by $\sigma_{w,k}^2 \in [\frac{1}{\rho}\sigma_{n,k}^2, \rho\sigma_{n,k}^2]$ where ρ is the corresponding NU parameter. Hence, the worst-case false alarm probability is expressed as follows:

$$\begin{aligned} P_{FA} &= \max_{\sigma_{w,k}^2 \in [\frac{1}{\rho}\sigma_{n,k}^2, \rho\sigma_{n,k}^2]} \mathcal{G}\left(\frac{\gamma - \left(\frac{\sigma_{w,k}^2}{2} + C\sqrt{\frac{6}{L_t}}\frac{\sigma_{w,k}^2}{\pi}\right)}{\left(\frac{6}{L_t}\right)^{1/4}\frac{\sigma_{w,k}}{\sqrt{\pi}}}\right) \\ &= \mathcal{G}\left(\frac{\gamma - \left(\frac{\rho\sigma_{n,k}^2}{2} + C\sqrt{\frac{6}{L_t}}\frac{\rho\sigma_{n,k}^2}{\pi}\right)}{\left(\frac{6}{L_t}\right)^{1/4}\sqrt{\frac{\rho}{\pi}}\sigma_{n,k}}\right), \end{aligned} \tag{23}$$

where ρ is corresponding uncertainty parameter. Based on Eq. (23), threshold is formulated as,

$$\gamma = \mathcal{G}^{-1}(P_{FA})\left(\frac{6}{L_t}\right)^{1/4}\sqrt{\frac{\rho}{\pi}}\sigma_{n,k} + \frac{\rho\sigma_{n,k}^2}{2} + C\sqrt{\frac{6}{L_t}}\frac{\rho\sigma_{n,k}^2}{\pi}. \tag{24}$$

[1] The detailed analysis is provided in the "Appendix."

4.2.2 Probability of detection

Similarly, detection probability is derived for $\mathcal{H}_1$ hypothesis from Eq. (18) as follows,

$$P_D = \min_{\sigma^2_{w,k} \in [\frac{1}{\rho}\sigma^2_{n,k}, \rho\sigma^2_{n,k}]} \mathcal{G}\left(\frac{\gamma - \left(\frac{\kappa}{2} + C\sqrt{\frac{6}{L_t}}\frac{\kappa}{\pi}\right)}{\left(\frac{6}{L_t}\right)^{1/4}\frac{\kappa}{\sqrt{\pi}}}\right) = \mathcal{G}\left(\frac{\gamma - \left(\frac{\widehat{\kappa}}{2} + C\sqrt{\frac{6}{L_t}}\frac{\widehat{\kappa}}{\pi}\right)}{\left(\frac{6}{L_t}\right)^{1/4}\sqrt{\frac{\rho}{\pi}}\widehat{\kappa}}\right) \tag{25}$$

where $\kappa = E_{max} - E_{min} + \sigma^2_{w,k}$ and $\widehat{\kappa} = E_{Max} - E_{Min} + \sigma^2_{n,k}/\rho$. E_{max} and E_{min} are evaluated as $E_{max} = \underset{k}{max}\left(|H_k|^2 E_k\right)$ and $E_{min} = \underset{k}{min}\left(|H_k|^2 E_k\right)$. H_k and E_k are PU channel gain and PU signal energy in subband k.

NU introduces severe effects in basic ED-based spectrum sensing methods. Since the observed primary signal PSD is frequency dependent and the noise is additive white Gaussian noise, the proposed maximum–minimum approach eliminates the noise floor. Removal of the noise floor minimizes the uncertainty effects, and hence, the proposed Max–Min-based CSS method is robust is to NU. Later, numerical results for the variation of the detection threshold γ based on Eq. (24) on the proposed Max–Min ED are shown in Sect. 5.2.

4.3 Cooperative maximum–minimum energy detection

Analytical detection and false alarm probabilities with Max–Min ED for an individual sensing station are obtained from Eqs. (25) and (23), respectively. Linear fusion rules are applied to combine the sensing results from the sensing stations, each of which applies the Max–Min ED. Here, linear fusion rules for hard decision combining are applied at FC using *AND rule*, *OR rule* and *Majority rule*. Details of these linear fusion rules have been covered in Sect. 2. Cooperative probabilities after implementation of linear fusion rules are obtained from Eqs. (1), (2), and (3).

5 Experimental results and discussion

This section is divided into two subsections to separate the numerical results for the basic FFT- and AFB-based CSS and Max–Min ED-based CSS under different channel environments and receiver non-ideality conditions. The two schemes are tested in the following subsections in specific scenarios with different system parameters.

5.1 Numerical results for FFT- and AFB-based methods

In the FFT- and AFB-based study, the potential spectral hole between two relatively strong OFDM or FBMC channels is illustrated in Fig. 3. We focus on two cases, one with a gap between two OFDM channels and another one between two FBMC channels. The results can be generalized to cases where the gap is between an OFDM channel and an FBMC channel. The spectrum leakage due to transmitter non-idealities can lead to eventually filling up this spectral gap and raising the false alarm rate of the spectrum sensing module.

We specifically focus on a spectrum use scenario with two active PU channels, which operate in the 2.4 GHz ISM band. This is an unlicensed frequency band which is utilized by various applications, including WLAN signals, cordless phones, Bluetooth wireless devices, and even microwave ovens. OFDM-based 802.11g-type WLANs, or 802.11g-like FBMC spectra are considered at 3rd and 8th WLAN channels. The adjacent PU spectra do not overlap each other, and a 5 MHz or 8 MHz spectral hole is available between the two channels in the OFDM and FBMC cases, respectively. The difference is due to wider guard-bands needed around the active subcarriers in the OFDM case. Both active signals are assumed to have the same power level, normalized to 0 dB in our scenario.

Additionally, it is assumed that in the false alarm test situation, there is no additional signal in the spectral hole. However, the spectrum sensing may give false alarms due to interference leakage from the adjacent PUs due to their nonlinearity. Obviously, this effect depends on the strength of the adjacent PU signal as observed at each sensing station. In the inband detection test situation, there is a weak inband PU signal in the spectrum gap between the WLAN or FBMC channels which, however, are not active in this test case. Notice that the presence of any adjacent channel interference would increase the detection probability. In both tests, we normalize the observed PU power to the noise power, using the SNR of a PU at the sensing station as a parameter characterizing the observed PU signal strength. In the following figures, "Adjacent PU SNR" and "Inband PU SNR" refer to the average PU SNR at the sensing stations, while the log-normal fading characterizes the variations of the PU power level at the sensing stations.

A smaller subband spacing of 81.5 kHz is used for spectrum sensing and CR transmissions, instead of the 312.5 kHz sub-carrier spacing of WLAN. This improves the spectral resolution of spectrum sensing and CR operation. The frequency window is chosen as $N_f = 5$ to increase the detection performance. Then, the effective sensing subband width is 407.5 kHz. For consistent comparison, the sensing is done over 5 MHz spectrum gap in both WLAN and FBMC cases, using 12 sensing subbands. In the inband detection test situation, a single subband is occupied by the PU. A SU reports the presence of a PU if the sensing threshold is exceeded in any of the subbands.

The required sample complexity for $P_D = 0.9$ and $P_{FA} = 0.1$ at the target SNR $= -5.08$ dB is determined with the aid of Eq. (8) in [5] as $N_t = 91$ for non-cooperative spectrum sensing of a single subband with AWGN channel as a reference case. The same sample complexity is considered in our CSS study and desired cooperative $P_{FA,t} = 0.1$ is assumed with all fusion rules in the absence of adjacent channel interference. The PA nonlinearity of adjacent PUs introduces interference leakage to the spectrum gap between the PUs, as illustrated in Fig. 3, and the width of the spectral hole is reduced.

As it is mentioned in details in Sect. 2, the number of sensors is determined as 8 in this study. When higher number of sensing stations is considered, the performance of CSS is not significantly improved, on the contrary, the computational complexity increases significantly in our simulation scenarios. Considering a practical trade-off between the complexity and performance, the number of sensing stations is selected as 8 based on experimental results. Due to the space limit, the sensing performance of different number of sensing stations is not shown in this study.

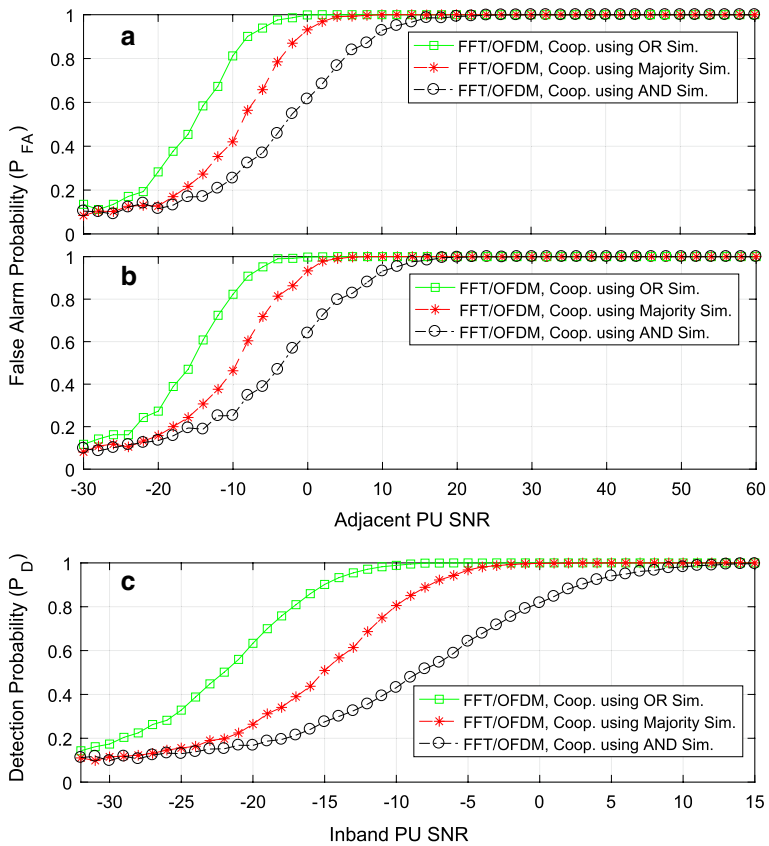

Fig. 5 Comparison of cooperative false alarm and detection probabilities between FFT-based SED for three different linear fusion rules under *Indoor* channel and log-normal fading ($\sigma = 9$ dB), time record length of $N_t = 91$, and $M = 8$ sensing stations. **a** P_{FA} with linear PA. **b** P_{FA} with nonlinear PA. **c** P_D for inband PU

Results from ideal and practical PA cases using the *Indoor* frequency selective channel for log-normal fading with standard deviation of $\sigma = 9$ dB are shown in Figs. 5 and 6 for the OFDM and FBMC cases, respectively. FBMC-based WLAN-like signal model shows much-improved spectral containment compared to OFDM-based WLAN under both the ideal and practical PA cases. Furthermore, AFB-based SED shows significant enhancement over the FFT-based one. Looking at the cooperative false alarm probability close to the target level of 0.1, the *AND rule* makes the CSS process least sensitive to interference leakage from the adjacent relatively strong PUs, while the *OR rule* shows highest sensitivity. This is true for both scenarios and both PA models. FBMC/OQAM with AFB-based SED is more robust towards the interference leakage from adjacent channels comparing with OFDM and FFT-based SED. With linear PA, the difference is quite significant, about 38 dB with all fusion rules as seen in Table 1. With the used highly nonlinear PA model, the difference is only 6–8 dB. On the other hand, *OR rule* gives the highest detection probability for inband PU signals. This confirms the observation [30] that "for many cases of practical interest," the *OR rule* delivers the best performance among hard-decision rules.

With FBMC waveform and AFB-based sensing, the *Majority rule* provides a reasonable trade-off between inband PU detection performance and robustness to interference

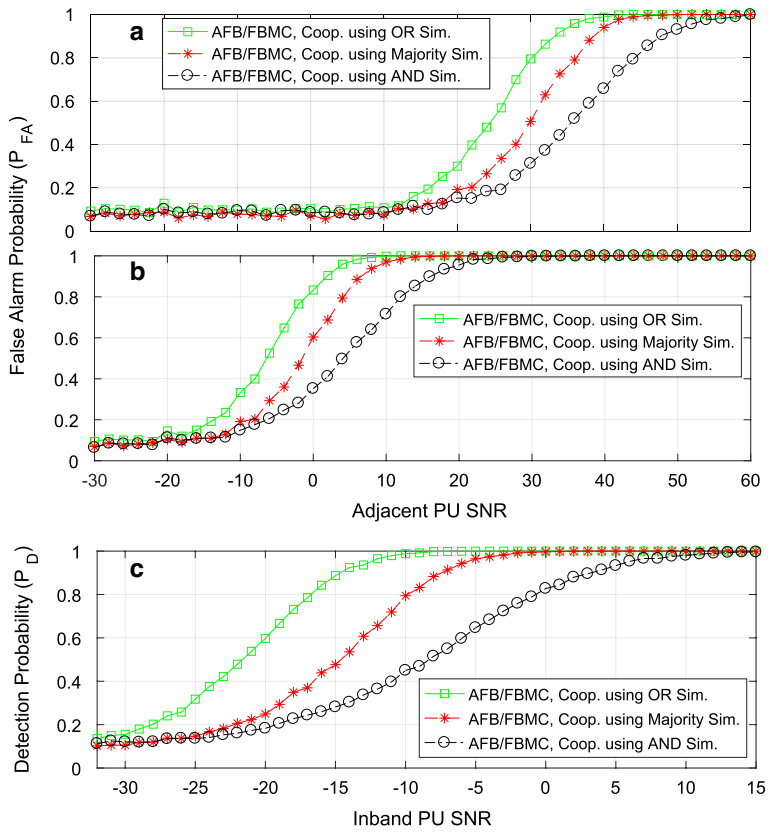

Fig. 6 Comparison of cooperative false alarm and detection probabilities between AFB-based SED for three different linear fusion rules under *Indoor* channel and log-normal fading ($\sigma = 9$ dB), time record length of $N_t = 91$, and $M = 8$ sensing stations. **a** P_{FA} with linear PA. **b** P_{FA} with nonlinear PA. **c** P_D for inband PU

Table 1 SNR requirements for inband and adjacent channel PU SNRs for $P_D \geq 0.9$ **and** $P_{FA} \leq 0.2$

	Min SNR of Inband PU (dB)	Max SNR of Adjacent PU	
		Linear PA (dB)	Nonlinear PA (dB)
OFDM/FFT—OR rule	− 15	− 22	− 22
—Maj rule	− 8	− 16	− 16
—AND rule	+ 3	− 12	− 12
FBMC/AFB—OR rule	− 15	+ 16	− 14
—Maj rule	− 8	+ 22	− 8
—AND rule	+ 3	+ 26	− 6

from adjacent channels. With linear PAs, the adjacent channels could have 30 dB higher SNR with respect to the sensing threshold. With the used nonlinear PA model and *Majority rule*, the average SNR of adjacent PUs should not exceed the SNR threshold of inband sensing, which severely limits in the sensing performance. We can conclude that, in order to make effective use of the good spectrum localization of FBMC waveform and AFB-based sensing in such scenarios, significantly better linearity for the PAs would be required with respect to the used nonlinear PA model.

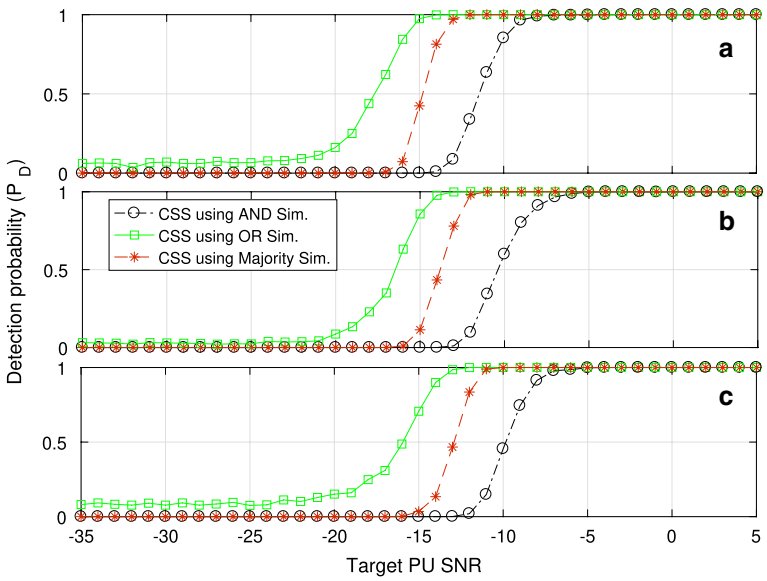

Fig. 7 CSS detection probabilities with **a** Max–Min ED, **b** Max/Min ED and **c** Diff. Max–Min ED and three different linear fusion rules for non-oversampled QPSK PU signal under *Indoor* channel and log-normal fading ($\sigma = 9$ dB), the length of $N_{FFT} = 8$, the number of sensing stations $M = 8$, the sample complexity $N = 10{,}240$, and 1 dB NU

5.2 Numerical results for Max–Min ED-based methods

The performance of the proposed novel Max–Min ED-based CSS and the comparison with traditional ED-based CSS are provided in this subsection. Proposed Max–Min ED-based CSS methods is considered here mainly in the 2x-oversampled signal cases. The main reason for the use of 2x-oversampled processing model is that it gives uncompromised sensing performance, while no oversampling or modest oversampling models give somewhat lower complexity at the cost of slightly reduced performance [7]. Results for non-oversampled case are also included for one of the scenarios. For the PU, we assume basic single-carrier signal with QPSK modulation at 20 MHz symbol rate. Assuming 20% roll-off in Nyquist pulse-shaping, the overall bandwidth is 24 MHz. In the non-oversampled case, the spectrum sensing process uses 20 MHz bandwidth between the 3-dB points of the transmitted spectrum, while in the 2x-oversampled case, the sensing bandwidth is extended to 40 MHz. In this study, the focus is on detection performance in the absence of strong interference effects, and the FFT- and AFB-based schemes provide quite similar results. For simplicity, we include only FFT-based schemes in this subsection, with two choices for the FFT length, 8 and 32.

The *Indoor* frequency selective channel [22] is assumed also here, along with the worst-case NU of 1-dB. The desired false alarm probability is chosen as $P_{FA} = 0.01$ for each station in all cases. The time record length is 10,240 QPSK symbols, i.e., 10,240 or 20,480 samples for non-oversamped and 2x oversampled cases, respectively. 1000 Monte Carlo simulations with different channel instances are applied to ensure the reliability of the simulation.

The number of sensing stations is selected as $M = 8$ for Max–Min ED-based CSS as well as it is explained in the previous section that number is determined based on the experimental results according to the trade of between the complexity and performance.

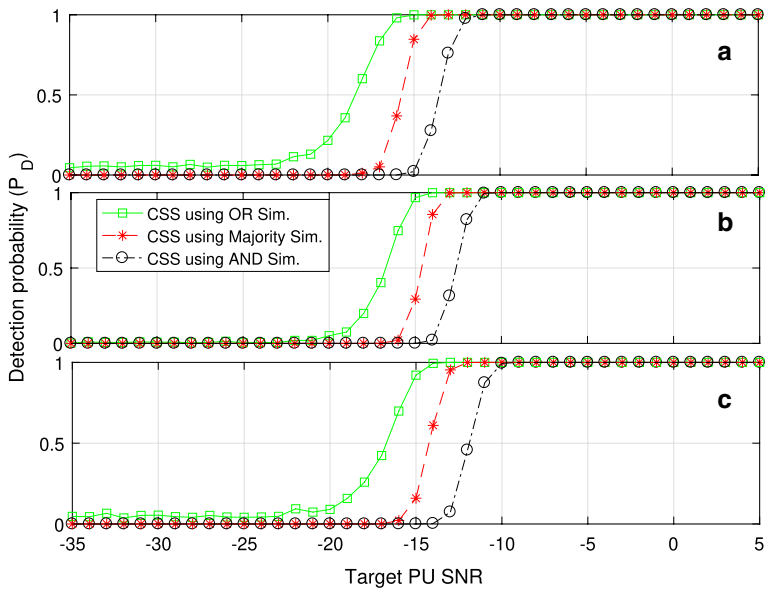

Fig. 8 CSS detection probabilities with **a** Max–Min ED, **b** Max/Min ED and **c** Diff. Max–Min ED and three different linear fusion rules for 2x-oversampled QPSK PU signal under *Indoor* channel and log-normal fading ($\sigma = 9$ dB), the length of $N_{FFT} = 8$, number of sensing stations $M = 8$, the sample complexity $N = 20{,}480$, and 1 dB NU

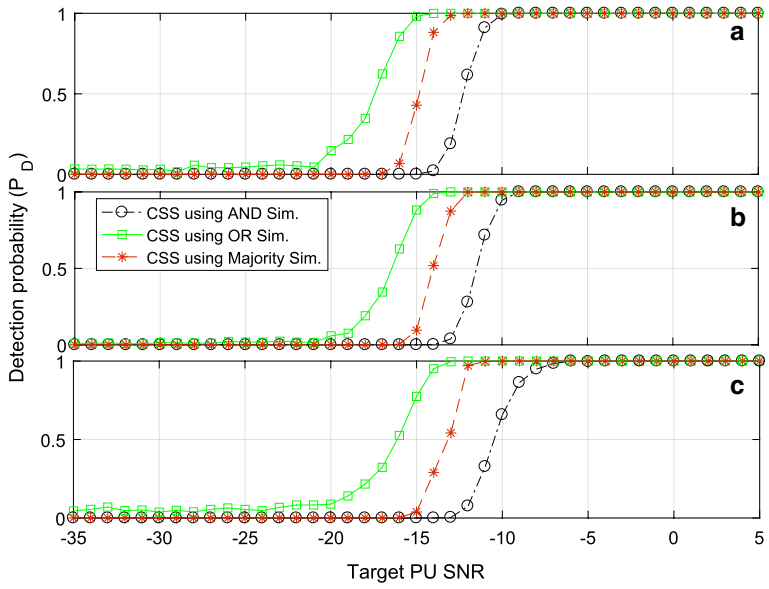

Fig. 9 CSS detection probabilities with **a** Max–Min ED, **b** Max/Min ED and **c** Diff. Max–Min ED and three different linear fusion rules for 2x-oversampled QPSK PU signal under *Indoor* channel and log-normal fading ($\sigma = 9$ dB), the length of $N_{FFT} = 32$, the number of sensing stations $M = 8$, the sample complexity $N = 20{,}480$, and 1 dB NU

There is no significant improvement on the sensing performance of Max–Min ED-based CSS approaches when the number of sensing stations is higher than 8.

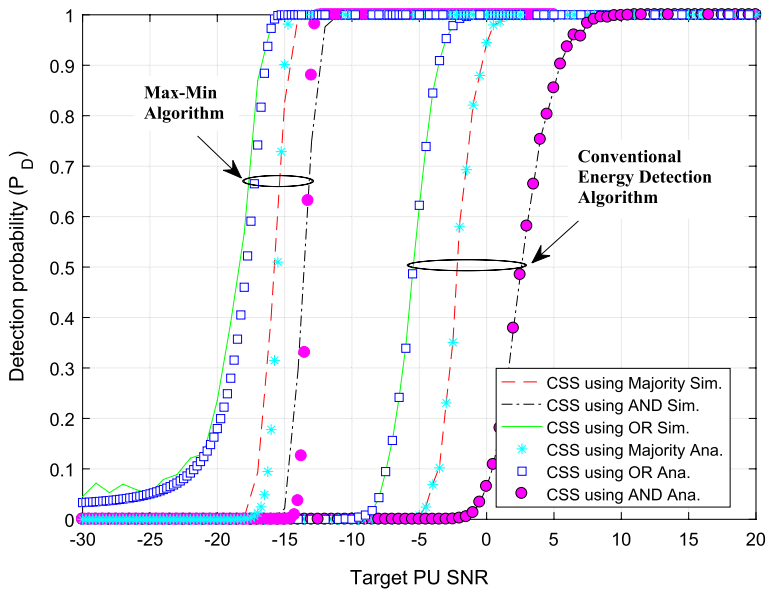

Fig. 10 Comparison of CSS detection probabilities between traditional ED and Max–Min ED with three different linear fusion rules for 2x-oversampled QPSK PU signal under *Indoor* channel and log-normal fading ($\sigma = 9$ dB), the length of FFT $N_{FFT} = 8$, the number of sensing stations $M = 8$, the sample complexity $N = 20{,}480$, and 1 dB NU

Three different CSS approaches, based on Max–Min ED, maximum/minimum ED (Max/Min ED), and differential Max–Min ED (Diff. Max–Min ED) are compared in Figs. 7, 8 and 9 with the two FFT lengths. Clearly, the *OR rule* gives the best detection performance in all cases. We can see that the cooperative Max–Min ED-based algorithm has in all tested cases better performance than the Differential Max–Min ED and Max/Min ED-based CSS algorithms. Hence, Max–Min ED-based CSS is proposed for the spectrum sensing purposes in this paper. Furthermore, the algorithm is simpler to implement and yet eliminates the noise floor thus reduces the uncertainty effects.

We can also see that the FFT length of 8 gives somewhat (about 1 dB) better sensitivity then the FFT length of 32 for all the three algorithms. Results for both non-oversampled and 2x-oversampled processing with FFT length of 8 are available in Figs. 7 and 8, indicating about 1 dB better sensitivity for the oversampled case. Similar differences were observed also in other tested scenarios. The reason for the difference is that in the non-oversampled case there are less variations in the ESD within the sensing bandwidth due to the PU signal, i.e., only 3 dB. Then, the frequency variability of ESD is mainly due to the frequency-selective channel.

Next, analytical results of proposed cooperative Max–Min ED are compared with simulation results in Figs. 10 and 11 for $N_{FFT} = 8$ and 32, respectively. Relatively good match between analysis and simulations can be seen in both cases.

In the same figures, the proposed cooperative Max–Min ED is compared with the traditional cooperative ED under the 1 dB NU condition. Both figures show that the proposed cooperative Max–Min ED clearly exceeds the performance of traditional cooperative ED in the presence of significant NU, which is yet realistic when considering practical receiver operation conditions. The proposed cooperative Max–Min ED has

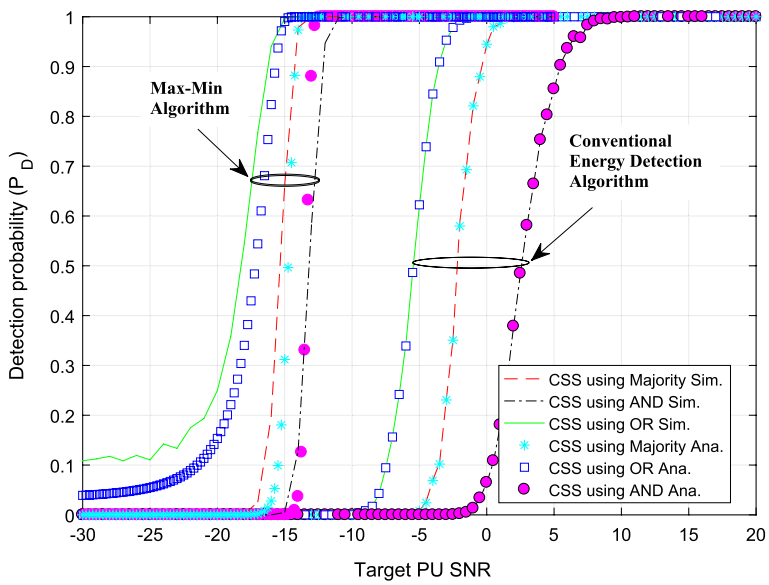

Fig. 11 Comparison of detection probabilities between traditional ED and Max–Min ED with three different linear fusion rules for 2x-oversampled QPSK PU signal under *Indoor* channel and log-normal fading ($\sigma = 9$ dB), the length of $N_{FFT} = 32$, the number of sensing stations $M = 8$, and the number of sampling complexity $N = 20{,}480$, and 1 dB NU

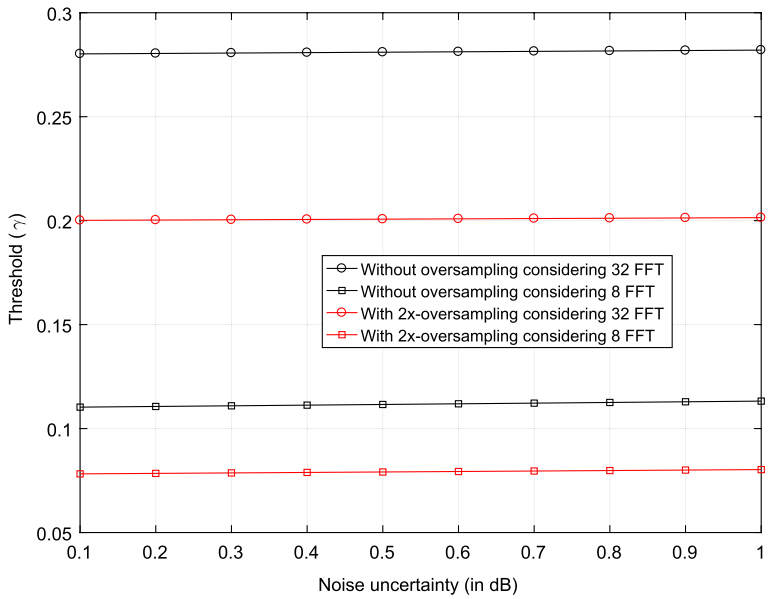

Fig. 12 Variation of the detection threshold γ of the proposed Max–Min ED for different NU values

approximately 10 dB better detection performance compared to traditional cooperative ED under the 1 dB NU condition.

Figure 12 shows the variation of the detection threshold γ (based on Eq. (24)) of the proposed Max–Min ED for non-oversampled and 2x-oversampled cases considering the

FFT lengths of 8 and 32 under different NU values between 0.1 and 1 dB. The threshold is quite independent of the NU, which can be seen as another indication of the robustness of this method.

The results of this subsection clearly demonstrate that *OR rule* is again the best in terms of detection performance. It should be noted that cooperative false alarm probability with Max–Min ED is independent of noise uncertainty and can be calculated using Eq. (1) as $P_{FA,t} = 0.077$ for the assumed $P_{FA} = 0.01$ of each sensing station.

6 Conclusion

In this paper, enhanced energy detection-based cooperative spectrum sensing methods were studied. In the first considered scenario, FFT- and AFB-based CSS was used to detect potential PU signals with widely varying bandwidths in possible spectral gaps close to strong PU channels. In such scenarios, the sensing task becomes difficult due to interference leakage from the relatively strong adjacent channels. The results demonstrated reduced sensitivity for filter bank-based waveforms and sensing schemes towards such interference leakage, compared to basic CP-OFDM and FFT-based sensing. However, for robust sensing in such scenarios, well linearized PAs are needed for the transmitters operating in the adjacent channels, in addition to using waveforms with good spectrum localization. As for the CSS schemes, it was found that the *Majority rule* provides a good trade-off between inband sensing performance and robustness to interference from adjacent channels. Also *k-out-of-M rules* with $1 < k \leq \mathrm{M}$ might be useful, depending on targeted detection and false alarm probabilities.

The second proposed scheme, Max–Min ED-based CSS is immune to NU effects and reduces the implementation complexity with respect to other schemes with similar robustness. This method utilizes the frequency variability of radio spectrum due to PUs. Maximum and minimum statistics were used to decide the presence or absence of PU signals with the help of predefined threshold. The Max–Min ED approach removes the noise floor from the signal that is additive in nature, which makes the algorithm stable to the NU effects. The proposed algorithm has reduced complexity compared to the eigenvalue-based approach [7]. The proposed method exhibited around 10 dB sensitivity enhancement for 1 dB NU condition in comparison with the traditional cooperative ED. Analytical performance evaluation was presented for the proposed algorithm and it matched well with the simulation results.

This study does not cover soft decision-based CSS, which remains as an important topic for future work.

Abbreviations

CR:: Cognitive radio; PU:: Primary user; AFB:: Analysis filter bank; CSS:: Cooperative spectrum sensing; FBMC:: Filter bank-based multicarrier; DWMT:: Discrete wavelet multitone; CMT:: Cosine modulated multitone; FMT:: Filtered multitone; OQAM:: Offset-QAM; ED:: Energy detection; SNR:: Signal to noise ratio; SU:: Secondary user; FFT:: Fast Fourier transform; PA:: Power amplifier; FC:: Fusion center; SED:: Subband energy detector; ADC:: Analog to digital converter; NU:: Noise uncertainty; Max–Min ED:: Maximum–minimum energy detector; Max/Min ED:: Maximum/minimum energy detector; Diff. Max–Min ED:: Differential maximum–minimum energy detector; 5G-NR:: Fifth generation new radio.

Acknowledgements

This work was supported in part by the Finnish Cultural Foundation.

Author Contributions

The idea, analysis, simulations, and writing were done with SD, KL, and MR. All authors read and approved the final manuscript.

Funding
This work was supported in part by the Finnish Cultural Foundation.

Availability of data and materials
Not applicable.

Competing interests
The authors declare that they have no competing interests.

Appendix

The details of closed-form expressions of Gumbel distribution

With the aid of (20) and (21), it is primarily essential to derive the expected value and standard deviation of the difference of maximum and minimum value. In what follows, we derive novel closed-form analytic expressions for these important measures which are subsequently used in deriving a comprehensive analytical framework for the proposed detector. It is firstly recalled that the nth moment of a continuous distribution with PDF $f(x)$ is defined as $E[x^n] = \int_{-\infty}^{\infty} x^n f(x)dx$ and the corresponding mean value is readily obtained for $n = 1$, i.e., $\mu = E[x]$. As a result, the mean value of (20) and (21) is given by $E[U_{\min}] = \int_{-\infty}^{\infty} x f_{\min}(x)dx$ and $E[U_{\max}] = \int_{-\infty}^{\infty} x f_{\max}(x)dx$, respectively, which yields $\mu_{\min} = E[U_{\min}] = -\alpha + \beta C$ and $\mu_{\max} = E[U_{\max}] = \alpha - \beta C$, where $C = 0.577215665$ is the Euler's constant. Consequently, the expected value of the difference of the maximum and minimum values is expressed as,

$$\mu_{\max-\min} = E[U_{\max-\min}] = 2\alpha - 2\beta C \tag{26}$$

and the location parameter can be determined by

$$\alpha = (E[U_{\max-\min}] + 2C\beta)/2. \tag{27}$$

Likewise, the corresponding variances are obtained by

$$\sigma^2_{\min} = \mathrm{Var}[\mathrm{U_{min}}] = \frac{1}{\beta}\int_{-\infty}^{\infty} (\mathrm{x} - \mathrm{E[U_{min}]})^2 \frac{\mathrm{e}^{\frac{\mathrm{x}-\mathrm{a}}{\beta}}}{\mathrm{e}^{\mathrm{e}^{\frac{\mathrm{x}-\mathrm{a}}{\beta}}}}\mathrm{dx} \tag{28}$$

and

$$\sigma^2_{\max} = \mathrm{Var}[\mathrm{U_{max}}] = \frac{1}{\beta}\int_{-\infty}^{\infty} (\mathrm{x} - \mathrm{E[U_{max}]})^2 \frac{\mathrm{e}^{-\frac{\mathrm{x}-\mathrm{a}}{\beta}}}{\mathrm{e}^{-\mathrm{e}^{\frac{\mathrm{x}-\mathrm{a}}{\beta}}}}\mathrm{dx} \tag{29}$$

which, unlike the mean values, are equivalent to each-other,

$$\mathrm{Var}[\mathrm{U_{min}}] = \mathrm{Var}[\mathrm{U_{max}}] = \frac{\pi^2\beta^2}{6}. \tag{30}$$

By recalling that $\mathrm{Var}(\mathrm{X} \pm \mathrm{Y}) = \mathrm{Var}(\mathrm{X}) + \mathrm{Var}(\mathrm{Y})$, when X and Y are mutually independent, it immediately follows that $\mathrm{Var}[\mathrm{U_{max}} - \mathrm{U_{min}}] = \mathrm{Var}[\mathrm{U_{max}}] + \mathrm{Var}[\mathrm{U_{min}}]$, which yields

$$\sigma^2_{\max-\min} = 2\mathrm{Var}[\mathrm{U_{max}}] = \frac{\pi^2\beta^2}{3} \tag{31}$$

and the scale parameter can be determined by

$$\beta = \sqrt{3\sigma^2_{U_{\max-\min}}}/\pi. \tag{32}$$

Received: 17 January 2020 Accepted: 16 December 2020
Published online: 15 February 2021

References

1. Federal Communications Commission. Spectrum policy task force. Report ET Docket no. 02-135, Nov (2002)
2. M. McHenry, Frequency agile spectrum access technologies. In *FCC Workshop on Cognitive Radio*, Washington, USA (2003)
3. S. Dikmese, S. Srinivasan, M. Shaat, F. Bader, M. Renfors, Spectrum sensing and spectrum allocation for multicarrier cognitive radios under interference and power constraints. EURASIP J. Adv. Signal Proc. **68** (2014)
4. S. Kandeepan, A. Giorgetti, Spectrum sensing in cognitive radio. In *Cognitive Radios and Enabling Techniques* (Artech House Publishers, Boston, 2012)
5. S. Dikmese, P.C. Sofotasios, T. Ihalainen, M. Renfors, M. Valkama, Efficient energy detection methods for spectrum sensing under non-flat spectral characteristics. IEEE J. Sel. Areas Commun. **33**(5), 755–770 (2015)
6. S. Dikmese, P.C. Sofotasios, M. Renfors, M. Valkama, Maximum–minimum energy based spectrum sensing under frequency selectivity for cognitive radios. In *Proceedings CROWNCOM'14 Conference*, Oulu, Finland (2014)
7. S. Dikmese, P.C. Sofotasios, M. Renfors, M. Valkama, Subband energy based reduced complexity spectrum sensing under noise uncertainty and frequency-selective spectral characteristics. IEEE Trans. Signal Process. **64**(1), 131–145 (2016)
8. S. Dikmese, Z. Ilyas, P.C. Sofotasios, M. Renfors, M. Valkama, Sparse frequency domain spectrum sensing and sharing based on cyclic prefix autocorrelation. IEEE J. Sel. Areas Commun. **35**(1), 159–172 (2017)
9. G. Ganesan, Y. Li, Cooperative spectrum sensing in cognitive radio, part I: two user networks. IEEE Trans. Wirel. Commun. **6**(6), 2204–2212 (2007)
10. A. Ali, W. Hamouda, Generalized FFT-based one-bit quantization system for wideband spectrum sensing. IEEE Trans. Commun. **68**(1), 82–92 (2020)
11. H. Sun, A. Nallanathan, S. Cui, C.X. Wang, Cooperative wideband spectrum sensing over fading channels. IEEE Trans. Veh. Technol. **65**(3), 1382–1394 (2016)
12. T. Yang, Y. Wu, L. Li, W. Xu, W. Tan, Fusion rule based on dynamic grouping for cooperative spectrum sensing in cognitive radio. IEEE Access **7**, 51630–51639 (2019)
13. J. Kim, J.P. Choi, Sensing coverage-based cooperative spectrum detection in cognitive radio networks. IEEE Sens. J. **19**(13), 5325–5332 (2019)
14. S. Dikmese, K. Lamichhane, M. Renfors, in *Novel Filter Bank Based Cooperative Spectrum Sensing Under RF Impairments and Channel Fading Beyond 5G Cognitive Radios*, eds. by A. Kliks, et al. Cognitive Radio-Oriented Wireless Networks. CrownCom 2019. Lecture Notes of the Institute for Computer Sciences, Social Informatics and Telecommunications Engineering, vol. 291 (Springer, Cham, 2019). https://doi.org/10.1007/978-3-030-25748-4_4
15. C. You, H. Kwon, J. Heo, Cooperative TV spectrum sensing in cognitive radio for Wi-Fi networks. IEEE Trans. Consum. Electron. **57**(1), 62–67 (2011)
16. P. Cheraghi, Y. Ma, R. Tafazolli, L. Zhengwei, Cluster-based differential energy detection for spectrum sensing in multi-carrier systems. IEEE Trans. Signal Process. **60**(11), 6450–6464 (2012)
17. S. Atapattu, C. Tellambura, H. Jiang, Energy detection based cooperative spectrum sensing in cognitive radio networks. IEEE Trans. Wirel. Commun. **10**(4), 1232–1241 (2011)
18. M.S. Hossain, M.I. Abdullah, Hard decision based cooperative spectrum sensing over different fading channel in cognitive radio. Int. J. Econ. Manag. Sci. **1**(1), 84–93 (2012)
19. S. Althunibat, M. Di Renzo, F. Granelli, Optimizing the K-out-of-N rule for cooperative spectrum sensing in cognitive radio networks. In *IEEE GLOBECOM'13*, pp. 1607–1611 (2013)
20. G. Bansal, J. Hossain, V.K. Bhargava, Adaptive power loading for OFDM-Based cognitive radio systems with statistical interference constraint. IEEE Trans. Wirel. Commun. **10**(9), 2786–2791 (2011)
21. Y. Cui, Z. Zhao, H. Zhang, An efficient filter banks based multicarrier system in cognitive radio networks. Radioengineering **19**(4), 479–487 (2010)
22. R. Jain, Channel models: a tutorial. In *WiMAX Forum AATG*, pp. 1–6 (2007)
23 E.J. Gumbel, Statistical theory of extreme values and some practical applications. Applied Mathematics Series 33, 1st edition. National Bureau of Standards, U.S. Department of Commerce (1954)
24. K.V. Burry, *Statistical Methods in Applied Science* (Wiley, Hoboken, 1975)
25. E. Castillo, *Extreme Value Theory in Engineering* (Academic Press Inc, New York, 1988)
26. S. Coles, *An Introduction to Statistical Modeling of Extreme Values* (Springer, London, 2001)
27. H.A. David, H.N. Nagaraja, *Order Statistics*. Wiley Series in Probability and Statistics, 3rd ed. (2003)
28. R.V. Mises, La distribution de la plus grande de n valeurs Rev. Math, Union Interbalkanique (1936)
29. H. Voss, A symmetry exploiting Lanzcos method for symmetric Toeplitz matrices. Numer. Algorithms **25**(4), 377–385 (2011)

30. A. Ghasemi, E.S. Sousa, Opportunistic spectrum access in fading channels through collaborative sensing. J. Commun. **2**(2), 71–82 (2007)

Publisher's Note